American Mineralogist, Volume 93, pages 1558–1567, 2008

Neutron diffraction study of δ-AlOOD at high pressure and its implication for symmetrization of the hydrogen bond

ASAMI SANO-FURUKAWA,[1,*] KAZUKI KOMATSU,[2,3] CARINE B. VANPETEGHEM,[4] AND EIJI OHTANI[1]

[1]Department of Earth and Planetary Materials Science, Tohoku University, Sendai 980-8578, Japan
[2]Geochemical Laboratory, Graduate School of Science, University of Tokyo, Tokyo 113-0033, Japan
[3]Centre for Science at Extreme Conditions, University of Edinburgh, Mayfield Road, Edinburgh, EH9 3JZ, U.K.
[4]School of Chemistry and Biochemistry, Georgia Institute of Technology, Atlanta, Georgia 30332, U.S.A.

ABSTRACT

We have conducted a powder neutron diffraction study of the distorted rutile-type hydrous phase δ-AlOO($D_{0.74}H_{0.26}$) at pressures up to 9.2 GPa. Rietveld refinement reveals that the observed diffraction data are best fitted by a model with an asymmetric hydrogen bond (space group $P2_1nm$). The Al-O2 bonds of the AlO_6 octahedron remain longer than the Al-O1 bonds up to 9.2 GPa, reflecting the fact that O2 is the donor and O1 is the acceptor of the hydrogen bond of O2-D···O1. As pressure increases, the Al-O1 bond lengths remain almost constant or increase slightly, whereas the longer Al-O2 bonds are more compressible. The O···O distance of the shared edge of the octahedron is almost constant unlike the other O···O distances that decrease during compression. The bulk modulus of the AlO_6 octahedron is determined to be 197.0(4) GPa, where K' is fixed to 4. The AlO_6 octahedron rotates about 1° during compression to 9.2 GPa. As pressure increases and the O2···O1 distance decreases, the D···O1 bond is shortened, whereas the O2-D bond becomes elongated, with pressure dependencies of $-1.81(9) \times 10^{-2}$ Å/GPa and $0.57(8) \times 10^{-2}$ Å/GPa, respectively, implying the symmetrization of the hydrogen bond at high pressure. The decrease in intensity of the 120 reflection as pressure increases suggests that the transition from the structure with space group $P2_1nm$ to that with $Pnnm$ would take place in δ-AlOOD at high pressure. This transition could be attributed to the disorder of deuterium or symmetrization of the hydrogen bond.

Keywords: δ-AlOOD, neutron diffraction, hydrogen bond, symmetrization

INTRODUCTION

It is widely recognized that the covalently bonded O-H distance correlates with the O···O distance of the O-H···O hydrogen bond geometry in various materials (e.g., Ichikawa 2000). In weak hydrogen bond systems consisting of O···O distances longer than 2.6 Å, the O-H distance is almost constant within the range of 0.95–1.0 Å. On the other hand, the O-H distance increases as the O···O distance decreases when the latter is shorter than 2.6 Å. The O-H distance reaches the straight line of $d_{O\text{-}H} = 1/2\ d_{OO}$ at the minimum O···O distance around 2.4 Å, where hydrogen is located at the center between two O atoms. This correlation is explained from the standpoint of the proton potential. The proton potential has two minima along the O···O line of the O-H···O geometry, but hydrogen is localized at one of them, forming an asymmetric hydrogen bond in the region of O···O distances longer than 2.6 Å. Since the potential barrier is lowered as O atoms come closer together, the proton is disordered between two potential minima when it can overcome the potential barrier by the tunneling effect or thermal vibration. Further decrease of the O···O distance turns the double potential well into a single minimum, and hydrogen is located at the midpoint between two O atoms. Following previous works, the term "symmetric hydrogen bond" is used to denote the proton-centered hydrogen bond geometry in this paper, although a disordered hydrogen bond is also crystallographically symmetric.

Applying pressure to the hydrogen bond also induces the decrease of O···O distances and the formation of a strong hydrogen bond. After the prediction of symmetrization of the hydrogen bond in ice by a theoretical study (Holzapfel 1972), many theoretical and experimental studies have been conducted to understand the pressure response of the hydrogen bond (e.g., Goncharov et al. 1996; Aoki et al. 1996; Benoit et al. 1998; Loubeyre et al. 1999; Pruzan et al. 2003). Goncharov et al. (1996) provided experimental evidence of symmetrization of the hydrogen bond in H_2O and D_2O ice by an infrared reflectance study. They reported the decrease to zero in the frequency of an OH-stretching mode of ice VII as pressure is increased to 60 GPa in H_2O and 70 GPa in D_2O. Above these pressures, a new lattice vibrational mode appears, which increases in frequency, suggesting the transformation from molecular crystal to atomic crystal. A neutron diffraction study is useful because neutrons are sensitive to hydrogen. However, pressure-induced symmetrization of the hydrogen bond in ice has not been directly observed by a neutron diffraction experiment because it requires a large amount of sample, which restricts the achievable pressure range.

δ-AlOOH is a high-pressure polymorph of diaspore (α-AlOOH) and boehmite (γ-AlOOH) (Suzuki et al. 2000). It is isostructural with guyanaite (β-CrOOH), the ICSD structure type, which has a distorted rutile-type structure. This hydrous phase has a wide stability field under lower mantle conditions,

---

* Present address: Institute for Solid State Physics, The University of Tokyo, Kashiwa 277-8581, Japan. E-mail: sano@issp.u-tokyo.ac.jp

0003-004X/08/0010–1558$05.00/DOI: 10.2138/am.2008.2849

indicating that it is a candidate for a carrier of hydrogen into the deep lower mantle (Ohtani et al. 2001; Sano et al. 2004, 2008). Suzuki et al. (2000) first synthesized δ-AlOOH at 21 GPa and 1000 °C and refined the structure by the Rietveld method without determining the hydrogen position. Based on the previous studies of $M^{3+}OOH$ hydroxide β-CrOOH (Christensen et al. 1976), they adopted the distorted rutile structure model with space group $P2_1nm$. The structure resembles $CaCl_2$-type SiO_2, a high-pressure polymorph of stishovite (e.g., Andrault et al. 1998); edge-sharing AlO_6 octahedra make a single chain along the *c* axis, and each chain connects to the next one via a corner. The hydrogen position of δ-AlOOH was investigated by single-crystal X-ray diffraction studies, but there is a disagreement in the results from two samples with slightly different chemical compositions. Komatsu et al. (2006) determined the space group of end-member δ-AlOOH as $P2_1nm$, in agreement with Suzuki et al. (2000). Their difference Fourier map shows a significant residual peak between O1 and O2 atoms in the tunnel formed by the octahedral chains. A short O···O distance of 2.548 Å suggests the presence of a strong hydrogen bond. On the other hand, Kudoh et al. (2004) reported two hydrogen positions in δ-$(Al_{0.84}Mg_{0.07}Si_{0.09})OOH$, from which the space group was determined to be $Pnn2$; one hydrogen position is the H1 site in the tunnel of the distorted rutile structure, and the other is the H2 site near the polyhedral edge. Raman and NMR studies of δ-AlOOH also indicated the existence of a strong hydrogen bond under ambient conditions (Xue et al. 2006).

δ-AlOOH has been the subject of theoretical studies by virtue of its unique features, such as a strong hydrogen bond, wide stability field, and structural similarity to stishovite. All of the theoretical studies performed thus far have predicted that a symmetric hydrogen bond would be formed in δ-AlOOH, although there is very little agreement about the pressure condition where the symmetrization takes place. Tsuchiya et al. (2002) reported that the second-order transition from the structure with an asymmetric hydrogen bond (space group $P2_1nm$) to that with a symmetric hydrogen bond ($Pnnm$) occurs at 28 GPa. They also suggested that the symmetrization of the hydrogen bond affects the axial compressibility along the direction of the hydrogen bond, resulting in the increase of the bulk modulus by about 20%. In contrast, Panero and Stixrude (2004) concluded that the symmetric hydrogen bond is stable even at ambient pressure, whereas Li et al. (2006) argued that the transition from asymmetric to symmetric hydrogen bond occurs at 50 GPa.

Very recently, we conducted a neutron diffraction experiment on deuterated δ-$AlOO(D_{0.744}H_{0.256})$ under ambient conditions to settle the issue of hydrogen bond geometry (Vanpeteghem et al. 2007). The observed diffraction pattern was best fitted by the model with the space group of $P2_1nm$ in the Rietveld refinement. The hydrogen bond geometry consists of an O2-D distance of 1.020 Å, a D···O1 distance of 1.552 Å, and an O2···O1 distance of 2.571 Å, suggesting that a strong but asymmetric hydrogen bond is formed in δ-AlOOD under ambient conditions. The present work presents an in situ observation of the pressure evolution of the strong hydrogen bond geometry in δ-AlOOD by neutron diffraction. Using these data, we discuss the compression mechanism and pressure-induced hydrogen bond symmetrization at high pressure in δ-AlOOD.

EXPERIMENTAL METHODS

Neutron-diffraction experiment at high pressure

The starting material for the neutron diffraction experiment was synthesized from deuterated bayerite $[Al(OD)_3]$ in 18 high-pressure experiments at 18 GPa and 900–1000 °C for durations of 30–60 min in a Kawai-type multi-anvil apparatus at Tohoku University. The same sample was used in a previous neutron study under ambient conditions (Vanpeteghem et al. 2007). Deuterated bayerite was obtained as a precipitate in a mixture of D_2O and $NaAlO_2$. The degree of deuteration was determined to be $AlOO[D_{0.744(2)}H_{0.256(2)}]$ by Rietveld refinement of the structure under ambient conditions. The contamination of hydrogen is probably due to the rapid exchange of deuterium for hydrogen in bayerite during storage and synthesis experiments. Time-of-flight (TOF) neutron powder diffraction experiments at high pressure were conducted at PEARL/HiPr diffractometer at the ISIS pulsed neutron source at the CCLRC Rutherford Appleton Laboratory, U.K. High pressure was achieved using a Paris-Edinburgh high-pressure cell with WC/Ni-binder anvils. The anvils were covered with cadmium foil to minimize the diffraction from the anvil materials. About 140 mg of powdered sample was loaded into a null-scattering TiZr alloy gasket (Marshall and Francis 2002). Deuterated methanol-ethanol (mixed 4:1 by volume) was used as a pressure medium to provide a hydrostatic condition. The sample tank in which the Paris-Edinburgh cell was installed was evacuated to prevent the influence of attenuation and scattering of the incident and scattered neutron beam. The diffraction pattern was collected using the 90° detector bank. Pressure was calculated from the unit-cell volume of δ-AlOOD at high pressure using a second-order Birch-Murnaghan equation of state for δ-AlOOH [$K = 152$ GPa and $K' = 4$ (fixed)] that was determined by a powder X-ray diffraction experiment using the data taken below 10 GPa (Kagi et al. 2006 and unpublished manuscript; Sano 2006). We note that disagreement remains about the equation of state of δ-AlOOH (Vanpeteghem et al. 2002; Tsuchiya et al. 2002; Panero and Stixrude 2004; Li et al. 2006; Kagi et al. 2006). The unit-cell volume of δ-AlOOD is shown in Table 1 so that recalculation is available if it becomes necessary in the future. The unit-cell volume obtained at 6 tons was used as V_0 to calculate the pressure. Neutron diffraction data were collected for 4–10 h at 11 different load conditions: 6, 15, 25, 35, 45, 55, 65, 75, 80, 85, and 90 tons, corresponding to 0.0001, 0.6, 2.0, 3.5, 4.7, 6.0, 7.0, 7.9, 8.4, 8.9, and 9.2 GPa, respectively. No significant broadening of diffraction peaks was observed to 9.2 GPa.

Rietveld refinement

The structure was refined by means of the Rietveld method (Rietveld 1969) using the General Structure Analysis System (GSAS) and the EXPGUI software package (Larson and Von Dreele 2004; Toby 2001). The occupancy of D and that of H of the hydrogen site were fixed to 0.744 and 0.266, which were determined by the previous study at ambient pressure (Vanpeteghem et al. 2007). The lattice constant, atomic position, isotropic displacement parameter, profile function, background function, and scale factor were refined using the TOF data with *d* value ranges from 0.4 to 4.27 Å. The isotropic displacement parameters are correlated to the apparent scattering length that correlates the site occupancy of hydrogen and deuterium during Rietveld refinements. Tungsten carbide (WC) and nickel were included in the refinement because a small number of diffraction peaks from the anvil were present in the pattern. A shifted Chebyschev function with 10 terms was used as the background function (function type 1; Larson and Von Dreele 2004), and an exponential pseudo-Voigt function (TOF function type 3; Larson and Von Dreele 2004) was used as a profile peak shape function.

RESULTS AND DISCUSSION

Structure model of δ-AlOOD

Theoretical studies have predicted that the hydrogen bond of δ-AlOOH becomes symmetric at high pressure (Tsuchiya et al. 2002; Li et al. 2006). Although there was no mention of the disorder of hydrogen in previous theoretical studies, the evolution of the hydrogen bond as a function of pressure should pass through the proton-disordered state before symmetrization, as in the case of ice. Therefore, we first compared the result of the Rietveld refinement based on three structural models defined as follows: (1) Hydrogen-Off-Centered (HOC)-I, an asymmetric hydrogen bond model (Fig. 1a, $P2_1nm$, a non-standard setting of space group $Pmn2_1$); (2) HOC-III, a fully disordered hydrogen bond

Table 1. Unit-cell parameters, density, and statistical measures of Rietveld refinements in the HOC-I model

Pressure	Lattice constants			Unit-cell volume	Density	R_{WP}*	R_P†	R_e‡	S§
(GPa)	a (Å)	b (Å)	c (Å)	(Å^3)	(g/cm^3)	(%)	(%)	(%)	
0	4.7179(2)	4.2361(2)	2.8323(1)	56.605(3)	3.563	2.86	4.61	2.22	1.29
0.6	4.7112(2)	4.2284(2)	2.8296(1)	56.368(3)	3.578	2.94	4.86	2.26	1.69
2.0	4.6969(2)	4.2133(2)	2.8243(1)	55.889(3)	3.609	2.91	4.81	2.28	1.28
3.5	4.6827(2)	4.1962(2)	2.8181(1)	55.374(3)	3.643	2.91	4.69	2.31	1.26
4.7	4.6706(2)	4.1836(3)	2.8129(1)	54.965(3)	3.670	3.03	4.92	2.34	1.29
6.0	4.6601(2)	4.1711(2)	2.8076(1)	54.574(3)	3.696	2.77	4.39	1.98	1.40
7.0	4.6506(2)	4.1610(2)	2.8033(1)	54.246(3)	3.718	2.66	4.59	2.05	1.30
7.9	4.6432(2)	4.1529(2)	2.8000(1)	53.992(3)	3.736	2.39	3.89	1.83	1.31
8.4	4.6393(2)	4.1477(2)	2.7978(1)	53.835(3)	3.747	2.42	3.93	1.85	1.31
8.9	4.6357(2)	4.1434(3)	2.7961(1)	53.705(3)	3.756	2.47	4.28	1.87	1.32
9.2	4.6328(2)	4.1401(3)	2.7947(1)	53.603(3)	3.763	2.32	3.74	1.73	1.34

* $R_{WP} = \Sigma_i|y_i - f_i(x)|/\Sigma_i y_i$.
† $R_P = \{\Sigma_i w_i[y_i - f_i(x)]^2/\Sigma_i w_i y_i^2\}^{1/2}$.
‡ $R_e = [N - P/\Sigma_i w_i y_i^2]^{1/2}$.
§ $S = R_{WP}/R_e$ where y_i = observed intensities; $f_i(x)$ = calculated intensities; w_i = statistical weight; N = Number of data points (2335); P = Number of parameters (36).

model (Fig. 1b, *Pnnm*); and (3) Hydrogen-Centered (HC), a symmetric hydrogen bond model (Fig. 1c, *Pnnm*). The names of the models use the nomenclature of the previous studies (Tsuchiya et al. 2002; Vanpeteghem et al. 2007). The starting parameters of the refinements are taken from the previous neutron diffraction study of δ-AlOOD under ambient conditions (Vanpeteghem et al. 2007) for the HOC-I model and β-CrOOH for the HOC-III and HC models (Fujihara et al. 2002). A previous theoretical study proposed the model named HOC-II (space group $Pn2_1m$), which has an asymmetric hydrogen bond with a different hydrogen position from HOC-I (Tsuchiya et al. 2002). Since the HOC-II model could not explain the observed neutron diffraction pattern at ambient conditions (Vanpeteghem et al. 2007), we did not take into account this model in the present study.

The observed and calculated diffraction patterns based on the HOC-I model at 9.2 GPa are shown in Figure 2. The R_{WP} values of the refinements using the HOC-I, HOC-III, and HC models were 2.86, 3.30, and 3.72 at 0.0001 GPa and 2.32, 2.43, and 2.54 at 9.2 GPa, respectively. As a result, the refinements based on the HOC-III and HC models resulted in a worsening of the quality of fit compared to the HOC-I model over the entire pressure range of the present study. Moreover, the 120 reflection was observed over the entire pressure range, which is explained only by the HOC-I model. At pressures above 7.9 GPa, it overlapped with the 101 reflection of WC, but it was still observed as a shoulder up to 9.2 GPa (Fig. 2). These results suggest that the hydrogen bond is neither symmetric nor fully disordered below 9.2 GPa. The unit-cell parameters and statistical measures of the refinements in the HOC-I model are summarized in Table 1, and the atomic positions and isotropic displacement parameters are presented in Table 2.

It is important to mention here that there is another structural model with space group of $P2_1nm$ in which deuterium is partially disordered between two sites along the O···O line of the hydrogen bond. Figure 3 shows difference Fourier maps synthesized from the difference between observed and refined structural factors, in which deuterium and hydrogen were removed. There were two peaks in the entire pressure range of the present study: a strong peak, here named Q1, corresponding to the deuterium site of the HOC-I model, and the other the weak peak Q2 near O1. This fact suggests the possibility of partial disorder of deuterium and hydrogen over two sites with

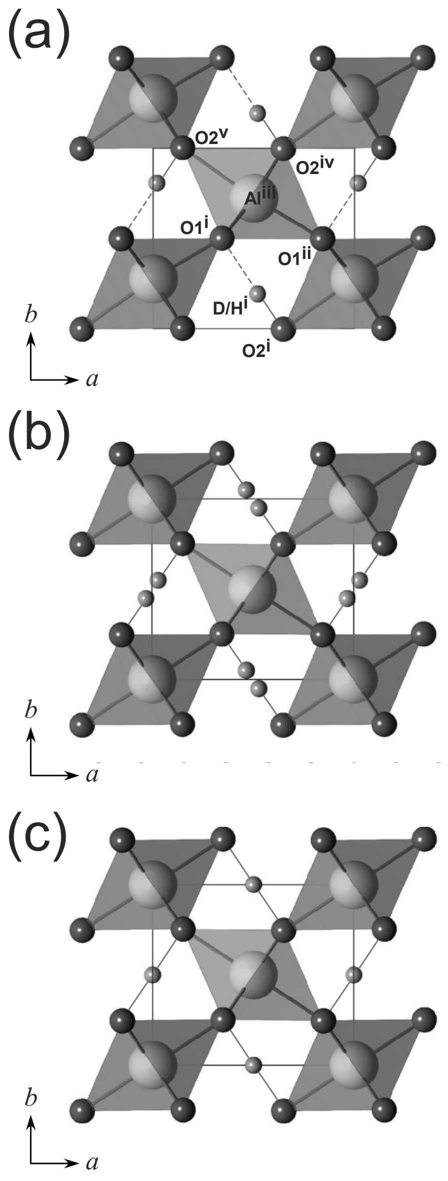

Figure 1. Structural models of δ-AlOOD. (**a**) HOC-I model, (**b**) HOC-III model, and (**c**) HC model. Roman figures in **a** are symmetry codes corresponding to those indicated in Table 4.

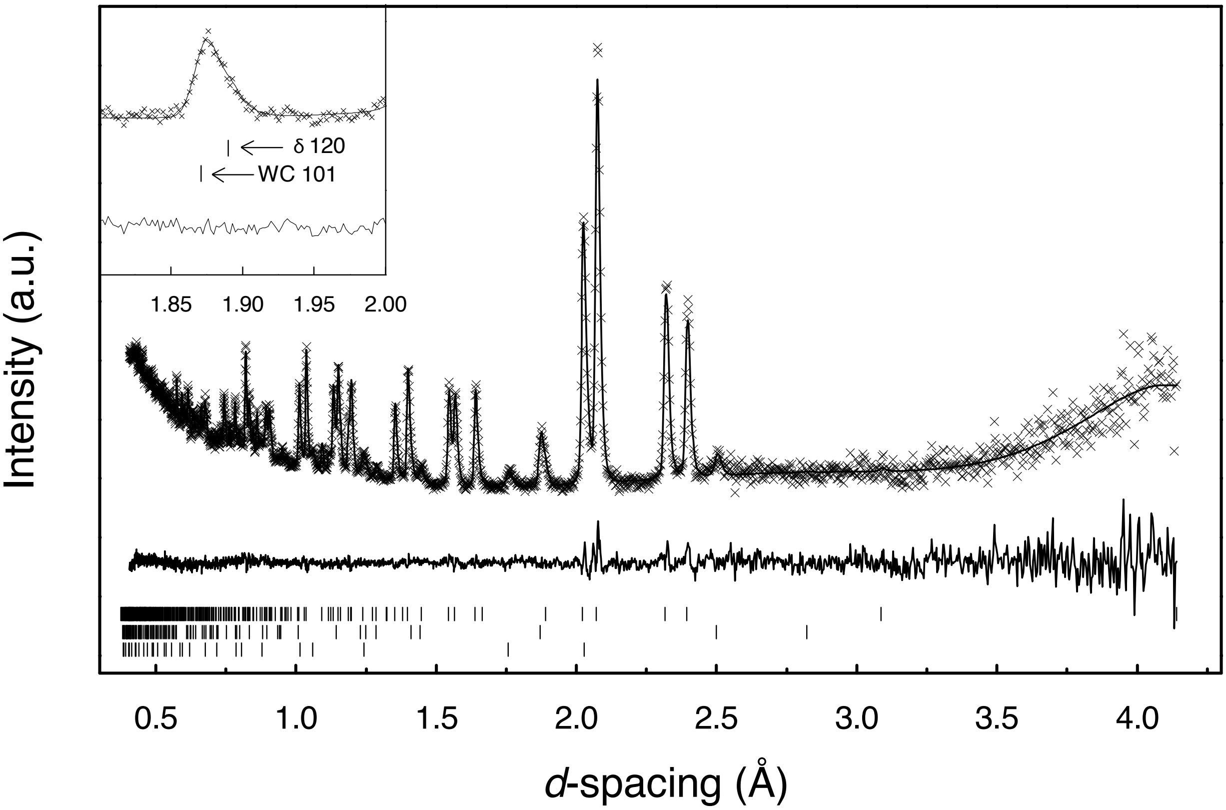

FIGURE 2. Observed neutron diffraction patterns (crosses), calculated and difference profiles (lines) of δ-AlOOD at 9.2 GPa. Vertical bars indicate the calculated peak positions of δ-AlOOD (top), Ni and WC (bottom). Inset figure shows the magnified pattern around the 120 reflection of δ-AlOOD at 1.89 Å.

different occupancies. The distances of O2-Q1 are almost the same or slightly longer than the O2-D distances of the HOC-I model, within the maximum difference of 0.06 Å. As pressure increases, the peak top value of Q2 increases and the separation of Q1-Q2 narrows in difference Fourier maps (Figs. 3a–3c). This probably indicates the lowering of the hydrogen potential barrier by compression, although the present study could not solve the detail of the evolution of deuterium distribution quantitatively because Rietveld refinement based on the partially disordered model ($P2_1nm$) failed to converge. This could be due to strong correlations in site occupancy, atomic position, and isotropic displacement parameter of deuterium and hydrogen between the two sites close to each other. If we tentatively distribute and fix the site occupancy of D1, D2, H1, and H2 according to the intensity ratio of residual peaks based on the assumption that deuterium and hydrogen occupy two sites with the same ratio, the refinement converges. The difference in the *R*-factor of the refinements of the results of the partially disordered model and the HOC-I model is negligible. The results of the refinement of the data obtained at 9.2 GPa, subject to the above constraints, are shown in Table 3. The compression behavior of δ-AlOOD is discussed based on the result of refinement with the HOC-I model hereafter.

AXIAL COMPRESSIBILITY

The compressibility of δ-AlOOD displays anisotropic behavior. Figure 4 shows the normalized axial compressibility of δ-AlOOD. The fit of the relationships between pressure and the cubic power of each cell edge with a second-order Birch-Murnaghan equation of state yields the bulk modulus of K_0 = 150.5 (4), 117.3 (1), and 214.6 (9) GPa for *a*, *b*, and *c*, respectively. The least compressible direction is *c*, down which the octahedral chains run, while the most compressible axis is *b*. Unlike the other two axes, which each show a distinctly non-linear response, the evolution of *c* is also well fitted using a linear function with $\beta_c = 4.085(7) \times 10^{-3}$ GPa^{-1}. This behavior is similar to that of stishovite, in which *c* is stiffer than *a* and is compressed linearly (Andrault et al. 2003). Tsuchiya et al. (2002) reported that the compressibility of each axis in δ-AlOOH differs between the HOC-I and HC models. Their results showed that *c* is less compressible than the *a* and *b* axes in the HOC-I model but becomes the most compressible direction in the HC model. The present result is in agreement with their theoretical study of the HOC-I model with an asymmetric hydrogen bond. No change in the axial compressibility was found up to 9.2 GPa in the present study.

Compression behavior of AlO_6 octahedron

The bulk modulus of an AlO_6 octahedron of δ-AlOOD shows the smallest reported value of the distorted rutile-type and rutile-type oxides. The rutile-type structure is described as follows. Half of the octahedral sites of a distorted hexagonal close-packed array of O atoms are occupied by a cation. In δ-AlOOD, deuterium is located in the other half of the octahedral sites, and

TABLE 2. Atomic positions and isotropic displacement parameters of δ-AlOOD at high pressure in the HOC-I model

Atom	Site	g*	*x*	*y*	*z*	U_{iso}×100 ($Å^2$)	Atom	Site	g*	*x*	*y*	*z*	U_{iso}×100 ($Å^2$)
0.0001 GPa							**7.0 GPa**						
Al	2*a*	1	0	0.277(1)	0	0.50(6)	Al	2*a*	1	0	0.270(1)	0	0.40(6)
O1	2*a*	1	0.339(2)	0.501(1)	0	0.53(2)	O1	2*a*	1	0.341(2)	0.493(1)	0	0.46(2)
O2	2*a*	1	0.645(2)	0.000(1)	0	0.53(2)	O2	2*a*	1	0.644(2)	0.004(1)	0	0.46(2)
D	2*a*	0.744	0.521(2)	0.191(1)	0	1.38(8)	D	2*a*	0.744	0.513(3)	0.207(1)	0	1.34(9)
H	2*a*	0.256	0.521(2)	0.191(1)	0	1.38(8)	H	2*a*	0.256	0.513(3)	0.207(1)	0	1.34(9)
0.6 GPa							**7. 9 GPa**						
Al	2*a*	1	0	0.274(1)	0	0.63(6)	Al	2*a*	1	0	0.267(1)	0	0.37(5)
O1	2*a*	1	0.339(2)	0.499(1)	0	0.53(2)	O1	2*a*	1	0.342(2)	0.494(1)	0	0.40(2)
O2	2*a*	1	0.643(2)	0.000(1)	0	0.53(2)	O2	2*a*	1	0.645(2)	0.005(1)	0	0.40(2)
D	2*a*	0.744	0.518(2)	0.194(1)	0	1.35(9)	D	2*a*	0.744	0.513(3)	0.209(1)	0	1.17(8)
H	2*a*	0.256	0.518(2)	0.194(1)	0	1.35(9)	H	2*a*	0.256	0.513(3)	0.209(1)	0	1.17(8)
2.0 GPa							**8.4 GPa**						
Al	2*a*	1	0	0.274(1)	0	0.39(6)	Al	2*a*	1	0	0.265(2)	0	0.43(5)
O1	2*a*	1	0.343(2)	0.498(1)	0	0.54(2)	O1	2*a*	1	0.347(2)	0.494(1)	0	0.42(2)
O2	2*a*	1	0.647(2)	0.001(1)	0	0.54(2)	O2	2*a*	1	0.648(2)	0.006(1)	0	0.42(2)
D	2*a*	0.744	0.522(2)	0.195(1)	0	1.18(8)	D	2*a*	0.744	0.517(3)	0.212(1)	0	1.30(8)
H	2*a*	0.256	0.522(2)	0.195(1)	0	1.18(8)	H	2*a*	0.256	0.517(3)	0.212(1)	0	1.30(8)
3.5 GPa							**8.9 GPa**						
Al	2*a*	1	0	0.271(1)	0	0.51(6)	Al	2*a*	1	0	0.265(2)	0	0.48(6)
O1	2*a*	1	0.341(2)	0.496(1)	0	0.51(2)	O1	2*a*	1	0.341(3)	0.492(1)	0	0.37(2)
O2	2*a*	1	0.645(2)	0.003(1)	0	0.51(2)	O2	2*a*	1	0.643(3)	0.007(1)	0	0.37(2)
D	2*a*	0.744	0.519(2)	0.198(1)	0	1.28(9)	D	2*a*	0.744	0.511(3)	0.215(1)	0	1.27(9)
H	2*a*	0.256	0.519(2)	0.198(1)	0	1.28(9)	H	2*a*	0.256	0.511(3)	0.215(1)	0	1.27(9)
4.7 GPa							**9.2 GPa**						
Al	2*a*	1	0	0.271(1)	0	0.52(6)	Al	2*a*	1	0	0.265(2)	0	0.46(5)
O1	2*a*	1	0.338(2)	0.498(1)	0	0.63(2)	O1	2*a*	1	0.343(3)	0.492(1)	0	0.38(2)
O2	2*a*	1	0.643(2)	0.004(1)	0	0.63(2)	O2	2*a*	1	0.646(3)	0.007(1)	0	0.38(2)
D	2*a*	0.744	0.517(2)	0.200(1)	0	1.49(10)	D	2*a*	0.744	0.513(3)	0.212(1)	0	1.28(8)
H	2*a*	0.256	0.517(2)	0.200(1)	0	1.49(10)	H	2*a*	0.256	0.513(3)	0.212(1)	0	1.28(8)
6.0 GPa													
Al	2*a*	1	0	0.270(1)	0	0.58(6)							
O1	2*a*	1	0.336(2)	0.495(1)	0	0.57(2)							
O2	2*a*	1	0.640(2)	0.003(1)	0	0.57(2)							
D	2*a*	0.744	0.515(2)	0.203(1)	0	1.46(9)							
H	2*a*	0.256	0.515(2)	0.203(1)	0	1.46(9)							

Notes: Space group $P2_1nm$. The isotropic atomic displacement parameters of oxygen, hydrogen, and deuterium were constrained to be $U_{iso}(O1) = U_{iso}(O2)$, $U_{iso}(H) = U_{iso}(D)$, and atomic positions of H and D were constrained to be the same. The occupancies of D and H were fixed to be the values determined at ambient conditions (Vanpeteghem et al. 2007).
* g = the fractional occupancy.

thus the structure could be described as a combination of AlO_6 and DO_6 octahedron. The octahedral volume of AlO_6 and DO_6 are almost the same under ambient conditions, but DO_6 is much more compressible than AlO_6, as expected (Table 4). The fit to a second-order Birch-Murnaghan equation of state leads to a bulk modulus of K_0 = 197.0(4) GPa for AlO_6, and K_0 = 124.9(3) GPa for DO_6. The bulk modulus of δ-AlOOD is much smaller than that of $CaCl_2$-type SiO_2 (K_0 = 311 GPa where K_0' = 4.95, Andrault et al. 1998) despite its similarity in structure. The polyhedral bulk moduli in the other rutile-type oxides are also greater than that of δ-AlOOD, 342 GPa with K' = 4 for stishovite (Ross et al. 1990) and 304 GPa with K' = 8 for GeO_2 (Haines et al. 2000).

Selected interatomic distances at each pressure are given in Table 4, and the compression behaviors of Al-O distances of the octahedron are plotted in Figure 5. In rutile-type and distorted rutile-type oxides, the octahedron is formed by four identical equatorial M-O bonds along the edge-sharing direction and two

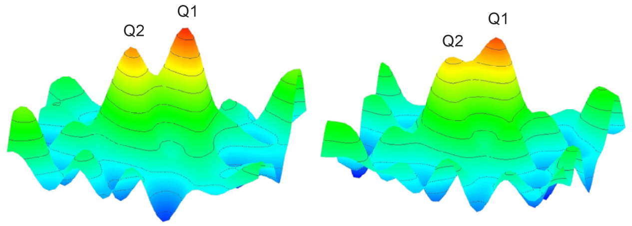

(a) 2.0 GPa (b) 7.0 GPa

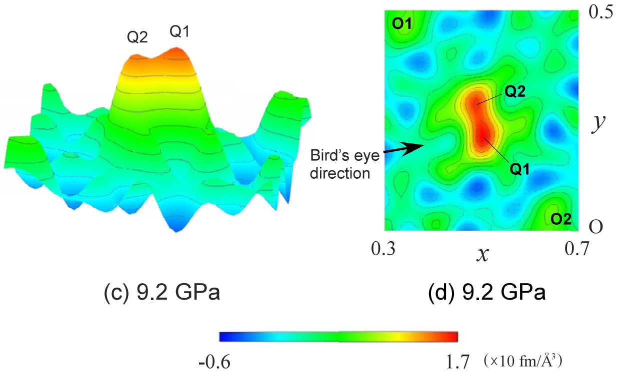

(c) 9.2 GPa (d) 9.2 GPa

◀**FIGURE 3.** Difference Fourier map synthesized from the difference between observed and refined structural parameters without deuterium and hydrogen. (**a–c**) Bird's eye views; (**d**) view from *c* axis.

TABLE 3. Summary of Rietveld refinement of data at 9.2 GPa using the partially disordered model

Result of Rietveld refinement of H-disordered model ($P2_1nm$)	
a (Å)	4.6327(2)
b (Å)	4.1402(3)
c (Å)	2.7947(1)
V (Å^3)	53.603(3)
Density (g/cm^3)	3.763
R_{WP}* (%)	2.31
R_P† (%)	3.73
R_e‡ (%)	1.73
S§ (%)	1.34

Atomic positions

Atom	Site	g‖	*x*	*y*	*z*	U_{iso}×100 (Å)
Al	2*a*	1	0	0.273(2)	0	0.25(6)
O1	2*a*	1	0.342(2)	0.491(2)	0	0.38(2)
O2	2*a*	1	0.645(2)	0.007(1)	0	0.38(2)
D1	2*a*	0.381	0.507(5)	0.197(3)	0	1.01(11)
H1	2*a*	0.134	0.507(5)	0.197(3)	0	1.01(11)
D2	2*a*	0.359	0.472(6)	0.273(5)	0	1.01(11)
H2	2*a*	0.126	0.472(6)	0.273(5)	0	1.01(11)

Hydrogen bond geometry

O2-D1 (Å)	1.01(2)	O2-D1···O1 (°)	172.9(9)
D1···O1 (Å)	1.44(2)	O1-D2···O2 (°)	177.8(10)
O1-D2 (Å)	1.08(3)	D1···D2 (Å)	0.36(3)
D2···O2 (Å)	1.36(3)		

Notes: The isotropic atomic displacement parameters were constrained to be U_{iso}(O1) = U_{iso}(O2), U_{iso}(D1) = U_{iso}(H1) = U_{iso} (D2) = U_{iso} (H2), and atomic positions of H1 and D1, H2 and D2 were constrained to be the same. The occupancies of H and D on the two hydrogen sites are fixed (see text).

* $R_{WP} = \Sigma_i|y_i - f_i(x)|/\Sigma_i y_{i}$.

† $R_P = \mathrm{TEM}\Sigma_i w_i[y_i - f_i(x)]^2/\Sigma_i w_i y_i^2\}^{1/2}$.

‡ $R_e = [N - P/\Sigma_i w_i y_i^2]^{1/2}$.

§ $S = R_{WP}/R_e$, where y_i, observed intensities; $f_i(x)$ = calculated intensities; w_i = statistical weight; *N* = number of data points (2335); *P* = number of parameters (38).

‖ g = the fractional occupancy.

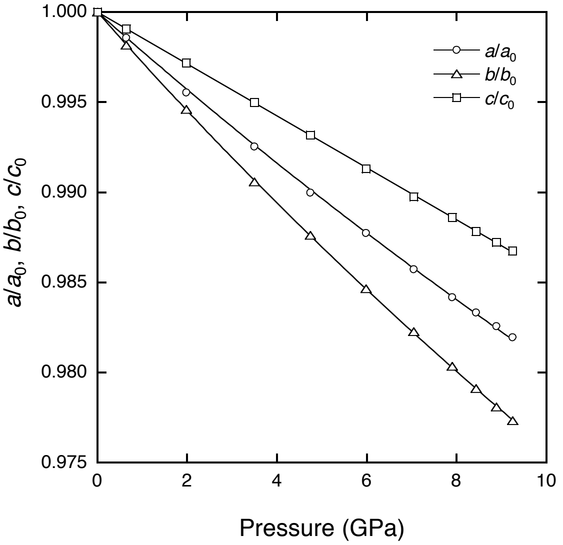

FIGURE 4. Pressure evolution of the normalized lattice constants of δ-AlOOD. The lines indicate the cubic root of the fit to a second-order Birch Murnaghan equation of state for $(a/a_0)^3$ and $(b/b_0)^3$ and a linear function for c/c_0. Error bars are smaller than the symbol size.

identical polar M-O bonds along the corner-linked direction. The equatorial bonds are less compressible than the polar bonds in both structures because equatorial bonds bridge between the repulsively interacting cations along the edge-sharing chain (Ross et al. 1990; Haines et al. 2000; Andrault et al. 1998). On the other hand, the aluminum ion is not located at the center of the AlO_6 octahedron of δ-AlOOD. The AlO_6 octahedron consists of four distinct bonds: (1) a polar Al-O2 bond, two equatorial Al-O2 bonds; (2) a polar Al-O1 bond; and (3) two equatorial Al-O1 bonds, in decreasing order of bond length. This feature is reasonable given the fact that O1 is the acceptor and O2 is the donor of the hydrogen bond. Since O2 is covalently bonded to deuterium forming a hydroxyl ion ($O2D^-$), O2 is slightly negatively charged compared to O1, and Al-O2 is longer than Al-O1. The main response to compression of the AlO_6 octahedron is the shortening of Al-O2 bonds, especially in the polar direction, whereas Al-O1 bonds remain almost constant or slightly increase. The equatorial Al-O1 bond remains shorter than the equatorial Al-O2 bond even at 9.2 GPa, suggesting that deuterium is neither fully disordered nor symmetric. If the D···O1 and

TABLE 4. Geometric parameters of δ-AlOOD at high pressure

Pressure (GPa)	0.0	0.6	2.0	3.5	4.7	6.0	7.0	7.9	8.4	8.9	9.2
AlO_6 octahedron*											
Al^{iii}-O1^{ii} (Å)	1.862(5)	1.859(9)	1.867(9)	1.867(10)	1.843(11)	1.825(10)	1.837(11)	1.845(11)	1.866(13)	1.838(13)	1.845(13)
Al^{iii}-O1^{i} [2] (Å)	1.860(8)	1.871(5)	1.861(5)	1.871(6)	1.867(6)	1.875(6)	1.867(6)	1.867(6)	1.862(7)	1.875(7)	1.869(7)
Al^{iii}-O2^{v} (Å)	2.044(8)	2.040(9)	2.016(9)	2.009(10)	2.010(10)	2.013(10)	1.992(10)	1.976(11)	1.954(13)	1.971(13)	1.957(13)
Al^{iii}-O2^{iv} [2] (Å)	1.963(4)	1.949(5)	1.951(5)	1.940(5)	1.934(6)	1.923(5)	1.927(6)	1.922(6)	1.923(7)	1.914(7)	1.919(7)
Al-O Average (Å)	1.925	1.923	1.918	1.916	1.909	1.906	1.903	1.900	1.898	1.898	1.896
O1^{i}-O2^{iv} [2] (Å)	2.561(8)	2.558(9)	2.555(9)	2.560(10)	2.550(10)	2.552(10)	2.551(10)	2.548(10)	2.546(12)	2.553(12)	2.555(6)
O1^{i}-O2^{v} [2] (Å)	2.705(6)	2.707(8)	2.700(7)	2.694(7)	2.677(8)	2.682(7)	2.680(7)	2.669(7)	2.665(9)	2.667(9)	2.662(8)
O1^{ii}-O2^{iv} [2] (Å)	2.701(6)	2.704(7)	2.694(7)	2.683(7)	2.685(8)	2.668(7)	2.661(7)	2.664(7)	2.666(9)	2.657(9)	2.656(8)
O1^{i}-O1^{ii} [2], O2^{v}-O2^{iv} [2] (Å)	2.751(10)	2.748(12)	2.740(11)	2.733(13)	2.726(13)	2.721(13)	2.716(13)	2.712(13)	2.710(20)	2.710(20)	2.706(6)
Volume (Å^3)	9.43(3)	9.40(4)	9.33(4)	9.28(4)	9.20(4)	9.16(4)	9.12(4)	9.08(4)	9.06(5)	9.06(5)	9.04(5)
Quad. elongation†	1.008(2)	1.007(2)	1.007(2)	1.006(2)	1.005(2)	1.006(2)	1.005(2)	1.005(2)	1.004(3)	1.004(3)	1.004(2)
Angle variance†	22.9	22.7	20.7	19.6	17.5	18.2	16.6	15.4	14.1	14.0	13.5
DO_6 octahedron											
Volume (Å^3)	9.44(3)	9.39(4)	9.30(4)	9.18(4)	9.12(4)	9.03(4)	8.96(4)	8.92(4)	8.88(5)	8.85(5)	8.82(5)
Hydrogen-bond geometry											
D···O1 (Å)	1.566(6)	1.545(6)	1.529(6)	1.504(6)	1.498(7)	1.472(6)	1.435(7)	1.426(6)	1.411(7)	1.393(7)	1.400(7)
O2-D (Å)	0.999(5)	1.009(5)	1.011(5)	1.008(5)	1.010(6)	1.019(6)	1.041(6)	1.042(5)	1.046(6)	1.058(7)	1.050(6)
O1···O2 (Å)	2.564(8)	2.553(9)	2.539(9)	2.511(10)	2.508(10)	2.491(10)	2.475(10)	2.468(10)	2.457(12)	2.450(12)	2.449(13)
O2-D···O1 (°)	177.1(5)	177.4(6)	177.6(5)	178.2(6)	178.5(6)	179.3(7)	178.2(6)	178.2(6)	178.5(6)	179.2(8)	178.2(7)

Note: Symmetry codes are as follows: i (*x*, *y*, 1 + *z*); ii (1/2 + *x*, 1 – *y*, 1/2 + *z*); iii (1/2 + *x*, 1 – *y*, 1/2 – *z*); iv (*x*, *y*, 1 + *z*); v (*x* – 1/2, 2 – *y*, *z* + 1/2).

* O1-O1, O2-O2 distances that are the same as the lattice constant of *c*, which is presented in Table 1.

† The quadratic elongation and angular variance of a regular polyhedron are 1.0 and 0.0, respectively (Robinson et al. 1971).

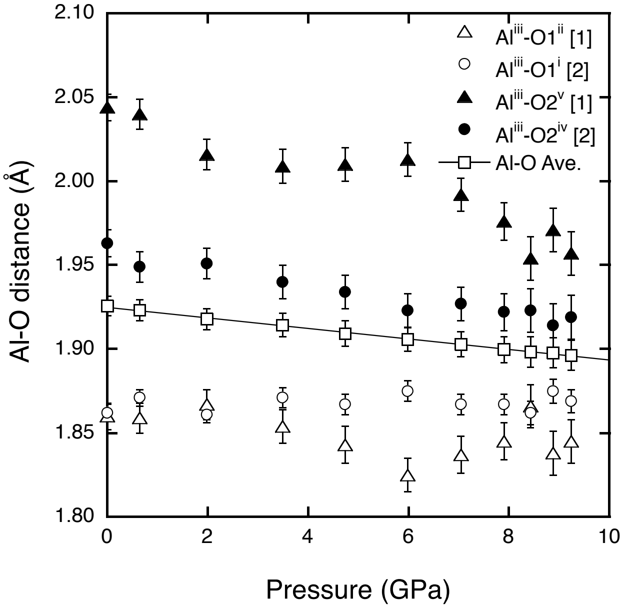

FIGURE 5. The Al-O distances of the AlO_6 octahedron of δ-AlOOD as a function of pressure. Symmetry codes are the same as those in Table 4. The solid line indicates the fit of the average Al-O distance using a linear equation.

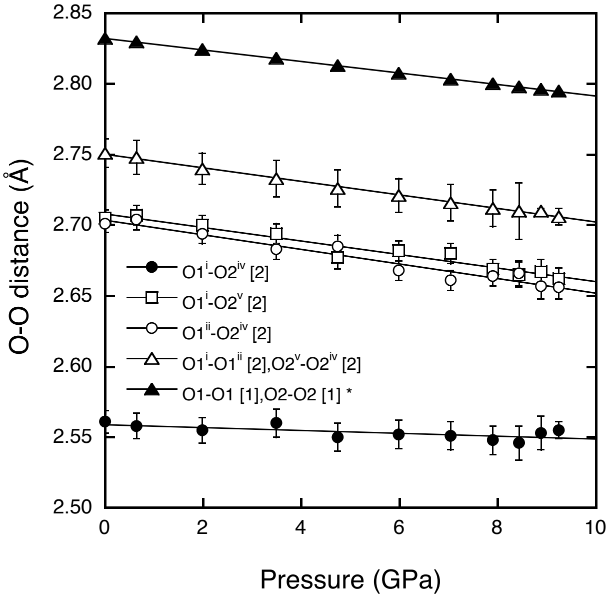

FIGURE 6. The O-O distances of the AlO_6 octahedron of δ-AlOOD as a function of pressure. The solid lines indicate the fit using a linear equation. Symmetry codes are the same as those in Table 4. * O-O distance along edge sharing chain, involving lattice constant *c*.

O2-D distances become equal by disorder or symmetrization of the hydrogen bond, the Al-O1 and Al-O2 bond lengths should be equal in both equatorial and polar directions and the space group should be *Pnnm*. The difference between Al-O1 and Al-O2 bond lengths tends to decrease at high pressure, and linear extrapolation leads to the expectation that the equatorial Al-O1 and Al-O2 bond lengths would be equal at 18.6 GPa.

The pressure response of the O···O distance of the edge of AlO_6 octahedra is shown in Figure 6. All O···O distances decrease with increasing pressure, except for the shortest one. The shortest O1-O2 distance that corresponds to a shared-octahedral edge remains almost constant within one standard deviation to 9.2 GPa. This response is similar to the compressibility of the octahedron of $CaCl_2$-type SiO_2 and GeO_2. Only the O···O distance of the shared octahedral edge increases with increasing pressure, whereas other O···O distances decrease (Haines et al. 2000; Andrault et al. 1998). The quadratic elongation (Robinson et al. 1971) of the AlO_6 octahedron remains almost constant in the range from 1.008(2) at ambient pressure to 1.004(2) at 9.2 GPa (Table 4).

Pressurization causes the rotation of the octahedron in the distorted rutile structure. The rotation of the octahedron is defined by the angles ω and ω' formed by twofold polar and equatorial axes of octahedra and diagonal lines of the unit cell in the *a*-*b* plane (Bärnighausen et al. 1984). In the *Pnnm* structure, the anion is located at the center of the octahedron and the cuboid that is formed by the eight surrounding cations defining the unit cell. The rotation angles of the octahedron in the rutile-type structure are geometrically calculated from the following equations:

$$\tan(45° + \omega) = b(0.5 - y)/a(0.5 - x)$$
$$\tan(45° - \omega') = by/ax,$$

where *x* and *y* are atomic positions of the anion. However, this equation could not be adapted to the δ-AlOOD structure that has the $P2_1nm$ space group. Here we redefine the rotation angle in δ-AlOOD, ω and ω', as angles formed by twofold axes of octahedra and lines connecting neighbor cations, as shown in Figure 7a. The angles are calculated based on the refined structural parameters using the VESTA software package (Momma and Izumi 2006). The rotation angles ω and ω' in δ-AlOOD are plotted in Figure 7b as a function of pressure. Both of the rotation angles of the octahedron increase about 1° from the value at ambient conditions with compression to 9.4 GPa. The rotation angle is smaller than those of other distorted rutile structures. For example, it increases from 3° at 1.0 GPa to 12° at 9.4 GPa in MnO_2 (Haines et al. 1995). Combining the result of the small rotation angle and bulk modulus of the AlO_6 octahedron compared to those of the other distorted rutile-type oxides, the predominant response to pressure in δ-AlOOD is concluded to be the compression of the octahedron rather than the rotation.

Pressure response of strong hydrogen bond

The pressure dependences of the hydrogen bond geometry are plotted in Figure 8. As pressure increases, the angle of the O2-D···O1 hydrogen bond increases slightly, from 176.3(2)° at ambient conditions to 178.2(7)° at 9.2 GPa. The O2···O1 and D···O1 distances of 2.564(8) and 1.566(6) Å at ambient pressure decrease to 2.449(13) and 1.400(7) Å at 9.2 GPa. At the same time, the O2-D bond length increases from 0.999(5) to 1.050(6) Å. If we assume linear correlations on the assumption that there is no change in compression behavior at high pressure, interatomic distances as a function of pressure are described as follows:

$$d_{O2O1}\ (\text{Å}) = 2.562(2) - 1.23(3) \times 10^{-2} \times P\ (\text{GPa}) \quad (1)$$

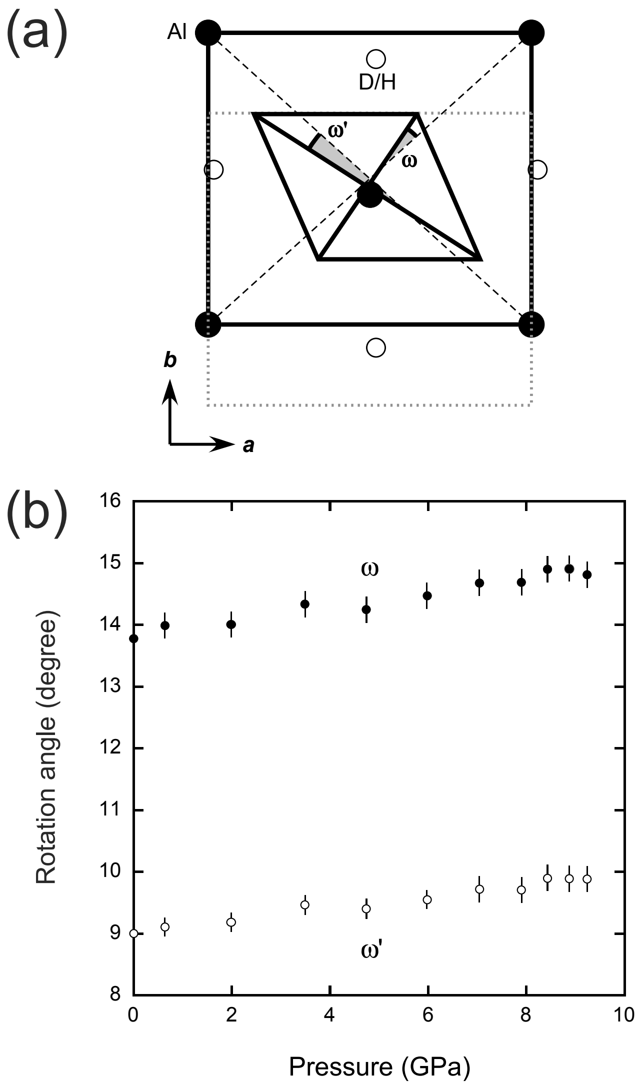

FIGURE 7. (**a**) Definition of the rotation angles ω and ω'. The dotted gray line is the unit cell; diamond-shaped figure is the AlO_6 octahedron. (**b**) Pressure evolution of rotation angle ω and ω' of the AlO_6 octahedra of δ-AlOOD.

$$d_{\mathrm{DO1}}\ (\text{Å}) = 1.567(5) - 1.81(9) \times 10^{-2} \times P\ (\text{GPa}) \quad (2)$$
$$d_{\mathrm{O2D}}\ (\text{Å}) = 0.996(5) + 0.57(8) \times 10^{-2} \times P\ (\text{GPa}) \quad (3)$$

The large variation in the O2-D distance of δ-AlOOD (0.57 × 10^{-2} Å GPa^{-1}) as a function of pressure is remarkable. Previous neutron diffraction studies of brucite, phase A, and chondrodite showed that the O-D distances are almost constant with pressure (Parise et al. 1994; Kagi et al. 2000; Friedrich et al. 2002). The pressure dependence of the O-D distance of D_2O ice VIII is also significantly lower (0.4 × 10^{-3} Å/GPa), which was determined by neutron diffraction at pressures up to 10 GPa, corresponding to O···O distances of 2.91 to 2.73 Å (Fig. 8, Nelmes et al. 1993). In δ-AlOOD, the AlO_6 framework restricts the O2···O1 distance to 2.56 Å at ambient pressure, which corresponds to the value in H_2O ice VII at 25 GPa [calculated using the equation of state of ice (Loubeyre et al. 1999) and the relationship $d_{\mathrm{OO}} = a \times (3/4)^{1/2}$, where a is the lattice constant]. This result suggests that the rate of increase of the covalent bond length as a function of pressure is significantly accelerated in the strong hydrogen bond system.

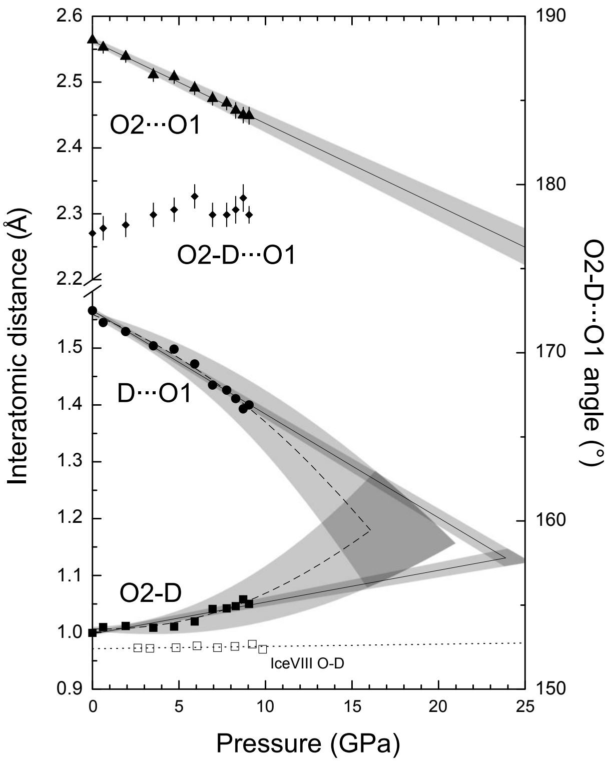

FIGURE 8. Pressure evolution of the hydrogen bond geometry of O2-D···O1 in δ-AlOOD and ice VIII (Nelmes et al. 1993). Error bars of O2-D and D···O1 distances are almost the same size as the symbol. The solid line and dashed curve indicate the fits using linear and second-order functions, respectively. Shaded areas indicate the error of the fit.

The linear extrapolations of O2-D and D···O1 evolutions cross at 24 GPa, which defines the symmetrization of the hydrogen bond (Fig. 8). However, the O2···O1 distance of 2.26 Å at 24 GPa calculated using Equation 1 is significantly shorter than expected. The relationship between O···O distance and O-H length in various materials confirms that the hydrogen reaches the centered position at an O···O length of 2.4 Å under ambient conditions (Ichikawa 2000). A theoretical calculation also predicted that pressure-induced symmetrization would take place at an O···O distance of 2.4 Å in δ-AlOOH and phase D (Tsuchiya et al. 2002, 2005). We could not rule out the possibility that linear extrapolation is not appropriate for strong hydrogen bond evolution and that symmetrization occurs at a lower pressure than 24 GPa because of an increasing rate of O-D expansion at high pressure. In the case of brucite, a theoretical study shows that O-H evolution as a function of O···O distance first increases linearly in the region of a weak hydrogen bond but responds nonlinearly as it strengthens (Mookherjee and Stixrude 2006). If we assume a second-order polynomial expression, the intersection of O2-D and D···O1 is located at 16 GPa, where O2···O1 is 2.37 Å (Fig. 8). The question of whether or not the critical O···O distance of pressure-induced symmetrization is the same as that under ambient conditions remains unsolved. Further investigation at high pressure is required.

The plots of O2-D distances as a function of O2···O1 distances are shown in Figure 9 together with a result of the previous theoretical study (Tsuchiya et al. 2002) and experimental studies of D_2O ice (Nelmes et al. 1993, 1998). The present study provides a shorter O-D distance than that of the theoretical calculation at the same O···O distance. There are many differences between theoretical and experimental studies, such as temperature and isotope (D and H) and we could not identify the reason for the discrepancy. It is likely that the correlation between O···O and O-D distances smoothly connects with previous neutron diffraction studies of D_2O ice VIII to 20 GPa (Nelmes et al. 1993, 1998). Extrapolated line of O2-D and O1···O2 distances using linear and non-linear equations are also plotted in Figure 9. Again we found that the variation of the O2-D distance is accelerated as the O2···O1 distance decreases, therefore symmetrization would take place at O···O distances longer than 2.26 Å, corresponding to pressures below 24 GPa.

Transformation of δ-AlOOD at high pressure

The 120 reflection observed around 1.90 Å at pressures below 9.2 GPa (Fig. 2) is explained only by the HOC-I model, whereas two models with the space group of *Pnnm* predict almost zero intensity. As shown in Figure 10, the intensity of the 120 reflection normalized by that of 111 continues to decrease at high pressure. It would decay to zero at 17.8 GPa if we adopt linear extrapolation, suggesting that the transformation from $P2_1nm$ to *Pnnm* occurs at this condition. There are two possible structural models in δ-AlOOD that take the space group of *Pnnm*; in one model, deuterium is completely disordered (HOC-III), whereas the other has a symmetric hydrogen bond (HC). As in the case of ice, compression of the hydrogen bond geometry would decrease the potential barrier, and deuterium would be disordered before symmetrization. Therefore, the transition could be attributed to the complete disorder of deuterium (HOC-III model) before symmetrization (HC model). There remains a certain degree of room for error in the transition pressure because it is based on an extrapolation. However, all the results of the pressure evolution of Al-O bond distances, hydrogen bond geometry, and the intensity of the 120 reflection indicate that hydrogen bond symmetrization would take place in δ-AlOOD at around 16–24 GPa.

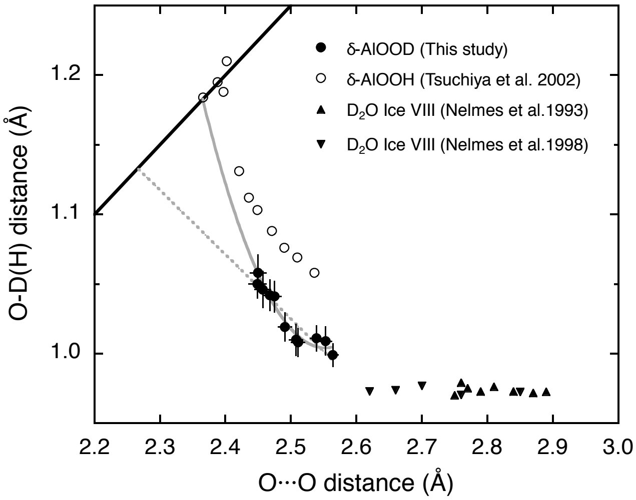

FIGURE 9. The evolution of the O-D distance as a function of O-O distance of δ-AlOOD. The solid bold line indicates the symmetrization line where the O-O distance is equal to twice the O-D distance. The dotted gray line and solid gray curve indicate the extrapolations using linear and second-order functions, respectively.

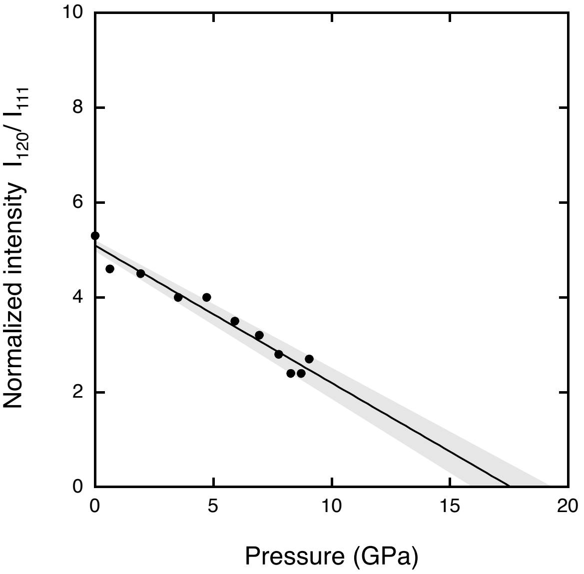

FIGURE 10. The change of intensity as a function of pressure of the 120 reflection of δ-AlOOD normalized by the intensity of the 111 reflection. The solid line indicates the fit using a linear equation and the shaded area indicates the error of the fit.

ACKNOWLEDGMENTS

We are grateful to W.G. Marshall, M.G. Tucker, and D.J. Francis for their technical support and helpful suggestions during the neutron diffraction experiments at ISIS. We thank T. Kondo, H. Kagi, and T. Kuribayashi for their critical comments and suggestions. Comments from an anonymous reviewer and M. Mookherjee greatly improved the manuscript. The crystal structure images in Figures 1 and 3 were drawn using VESTA developed by Momma and Izumi (2006). This work was partially supported by a Grant-in-Aid for Scientific Research to E.O. (no. 16340164) from the Ministry of Education, Culture, Sports, Science, and Technology of the Japanese Government, and was conducted as part of the 21st Century Center-of-Excellence program "Advanced Science and Technology Center for the Dynamic Earth." A.S. and K.K. were supported by Research Fellowships of the Japan Society for the Promotion of Science for Young Scientists.

REFERENCES CITED

Andrault, D., Fiquet, G., Guyot, F., and Hanfland, M. (1998) Pressure-induced Landau-type transition in stishovite. Science, 282, 720–724.

Andrault, D., Angel, R.J., Mosenfelder, J.L., and Bihan, T.L. (2003) Equation of state of stishovite to lower mantle pressures. American Mineralogist, 88, 301–307.

Aoki, K., Yamawaki, H., Sakashita, M., and Fujihisa, H. (1996) Infrared absorption study of the hydrogen-bond symmetrization in ice to 110 GPa. Physical Review B, 54, 15673–15677.

Bärnighausen, H., Bossert, W., and Anselment, B. (1984) A second-order phase transition of calcium bromide and its geometrical interpretation. IUCr 13th International Congress, Hamburg, Germany, 9–18 August 1984. Communicated abstracts, Acta Crystallographica Supplement, A40, C-96.

Benoit, M., Marx, D., and Parrinello, M. (1998) Tunneling and zero-point motion in high-pressure ice. Nature, 392, 258–261.

Christensen, A.N., Hansen, P., and Lehmann, M.S. (1976) Isotope effects in the bonds of β-CrOOH and β-CrOOD. Journal of Solid State Chemistry, 19, 299–304.

Friedrich, A., Lager, G.A., Ulmer, P., Kunz, M., and Marshall, W.G. (2002) High-pressure single-crystal X-ray and powder neutron study of F,OH/OD-chondrodite: Compressibility, structure, and hydrogen bonding. American

Mineralogist, 87, 931–939.

Fujihara, T., Ichikawa, M., Gustafsson, T., Olovsson, I., and Tsuchida, T. (2002) Powder-neutron diffraction studies of geometric isotope and hydrogen-bonding effects in β-CrOOH. Journal of Physics and Chemistry of Solids, 63, 309–315.

Goncharov, A.F., Struzhkin, V.V., Somayazulu, M.S., Hemley, R.J., and Mao, H.K. (1996) Compression of ice to 210 gigapascals: Infrared evidence for a symmetric hydrogen-bonded phase. Science, 273, 218–220.

Haines, J., Léger, J.M., and Hoyau, S. (1995) Second-order rutile-type to $CaCl_2$-type phase transition in β-MnO_2 at high pressure. Journal of Physics and Chemistry of Solids, 56, 965–973.

Haines, J., Léger, J.M., Chateau, C., and Pereira, A.S. (2000) Structural evolution of rutile-type and $CaCl_2$-type germanium dioxide at high pressure. Physics and Chemistry of Minerals, 27, 575–582.

Holzapfel, W.B. (1972) On the symmetry of the hydrogen bonds in ice VII. The Journal of Chemical Physics, 56, 712–715.

Ichikawa, M. (2000) Hydrogen-bond geometry and its isotope effect in crystals with OHO bonds—revisited. Journal of Molecular Structure, 552, 63–70.

Kagi, H., Parise, J.B., Cho, H., Rossman, G.R., and Loveday, J.S. (2000) Hydrogen bonding interactions in phase A [$Mg_7Si_2O_8(OH)_6$] at ambient and high pressure. Physics and Chemistry of Minerals, 27, 225–233.

Kagi, H., Sano, A., Fukura, S., Nakano, S., Nagai, T., Ohishi, Y., and Ohtani, E. (2006) Compression behavior of delta-AlOOH and experimental observation of the hydrogen bond symmetrization at high pressure. American Geophysical Union, Fall Meeting 2006, abstract no. MR11A-0100.

Komatsu, K., Kuribayashi, T., Sano, A., Ohtani, E., and Kudoh, Y. (2006) Redetermination of the high-pressure modification of AlOOH from single-crystal synchrotron data. Acta Crystallographica, E62, i216–i218.

Kudoh, Y., Kuribayashi, T., Suzuki, A., Ohtani, E., and Kamada, T. (2004) Space group and hydrogen sites of δ-AlOOH and implications for a hypothetical high-pressure form of $Mg(OH)_2$. Physics and Chemistry of Minerals, 31, 360–364.

Larson, A.C. and Von Dreele, R.B. (2004) General structure analysis system (GSAS). Los Alamos National Laboratory Report LAUR 86-748.

Loubeyre, P., LeToullec, R., Wolanin, E., Hanfland, M., and Hausermann, D. (1999) Modulated phases and proton centering in ice observed by X-ray diffraction up to 170 GPa. Nature, 397, 503–506.

Li, S., Ahuja, R., and Johansson, B. (2006) The elastic and optical properties of the high-pressure hydrous phase δ-AlOOH. Solid State Communications, 137, 101–106.

Marshall, W.G. and Francis, D.J. (2002) Attainment of near-hydrostatic compression conditions using the Paris-Edinburgh cell. Journal of Applied Crystallography, 35, 122–125.

Momma, K. and Izumi, F. (2006) An integrated three-dimensional visualization system VESTA using wxWidgets. Commission on Crystallographic Computing, IUCr Newsletter, 7, 106–119.

Mookherjee, M. and Stixrude, L. (2006) High-pressure proton disorder in brucite. American Mineralogist, 91, 127–134.

Nelmes, R.J., Loveday, J.S., Wilson, R.M., Besson, J.M., Pruzan, Ph., Klotz, S., Hamel, G., and Hull, S. (1993) Neutron diffraction study of the structure of deuterated ice VIII to 10 GPa. Physical Review Letters, 71, 1192–1195.

Nelmes, R.J., Loveday, J.S., Marshall, W.G., Besson, J.M., Klotz, S., and Hamel, G. (1998) Structures of Ice VII and Ice VIII to 20 GPa. The Review of High Pressure Science and Technology, 7, 1138–1140.

Ohtani, E., Litasov, K., Suzuki, A., and Kondo, T. (2001) Stability field of new hydrous phase, δ-AlOOH, with implications for water transport into the deep mantle. Geophysical Research Letters, 28, 3991–3993.

Panero, W.R. and Stixrude, L.P. (2004) Hydrogen incorporation in stishovite at high pressure and symmetric hydrogen bonding in δ-AlOOH. Earth and Planetary Science Letters, 221, 421–431.

Parise, J.B., Leinenweber, K., Weidner, D.J., Tan, K., and Von Dreele, R.B. (1994) Pressure-induced H bonding: Neutron diffraction study of Brucite, $Mg(OD)_2$, to 9.3 GPa. American Mineralogist, 79, 193–196.

Pruzan, Ph., Chervin, J.C., Wolanin, E., Canny, B., Gauthier, M., and Hanfland, M. (2003) Phase diagram of ice in the VII-VIII-X domain. Vibrational and structural data for strongly compressed ice VIII. Journal of Raman Spectroscopy, 34, 591–610.

Rietveld, H.M. (1969) A profile refinement method for nuclear and magnetic structures. Journal of Applied Crystallography, 2, 65–71.

Robinson, K., Gibbs, G.V., and Ribbe, P.H. (1971) Quadratic elongation: A quantitative measure of distortion in coordination polyhedra. Science, 172, 567–570.

Ross, N.L., Shu, J., Hazen, M.R., and Gasparik, T. (1990) High-pressure crystal chemistry of stishovite. American Mineralogist, 75, 739–747.

Sano, A. (2006) Phase relations and physical properties of δ-AlOOH at high pressure. Ph.D. thesis, Tohoku University, Sendai, Japan.

Sano, A., Ohtani, E., Kubo, T., and Funakoshi, K. (2004) In situ X-ray observation of decomposition of hydrous aluminum silicate $AlSiO_3OH$ and aluminum oxide hydroxide δ-AlOOH at high pressure and temperature. Journal of Physics and Chemistry of Solids, 65, 1547–1554.

Sano, A., Ohtani, E., Kondo, T., Hirao, N., Sakai, T., Sata, N., Ohishi, Y., and Kikegawa, T. (2008) Aluminous hydrous mineral δ-AlOOH as a carrier of hydrogen into the core-mantle boundary. Geophysical Research Letters, 35, L03303.

Suzuki, A., Ohtani, E., and Kamada, T. (2000) A new hydrous phase δ-AlOOH synthesized at 21 GPa and 1000 °C. Physics and Chemistry of Minerals, 27, 689–693.

Toby, B.H. (2001) EXPGUI, a graphical user interface for GSAS. Journal of Applied Crystallography, 34, 210–213.

Tsuchiya, J., Tsuchiya, T., Tsuneyuki, S., and Yamanaka, T. (2002) First principles calculation of a high-pressure hydrous phase, δ-AlOOH. Geophysical Research Letters, 29, 1909.

Tsuchiya, J., Tsuchiya, T., and Tsuneyuki, S. (2005) First-principles study of hydrogen bond symmetrization of phase D under high pressure. American Mineralogist, 90, 44–49.

Vanpeteghem, C.B., Ohtani, E., and Kondo, T. (2002) Equation of state of the hydrous phase δ-AlOOH at room temperature up to 22.5 GPa. Geophysical Research Letters, 29, 1119.

Vanpeteghem, C.B., Sano, A., Komatsu, K., Ohtani, E., and Suzuki, A. (2007) Neutron diffraction study of aluminous hydroxide δ-AlOOD. Physics and Chemistry of Minerals, 34, 657–661.

Xue, X., Kanzaki, M., Fukui, H., Ito, E., and Hashimoto, T. (2006) Cation order and hydrogen bonding of high-pressure phases in the Al_2O_3-SiO_2-H_2O system: An NMR and Raman study. American Mineralogist, 91, 850–861.

Manuscript received November 9, 2007
Manuscript accepted March 15, 2008
Manuscript handled by Ian Swainson